Viscosity calculation of a nanoparticle suspension confined in nanochannels

Yan Wang,[1,*] Pawel Keblinski,[2] and Zhenqian Chen[1]
[1]*School of Energy and Environment, Southeast University, Nanjing 210096, China*
[2]*Department of Materials Science and Engineering, Rensselaer Polytechnic Institute, Troy, New York 12180-3590, USA*
(Received 29 March 2012; revised manuscript received 23 July 2012; published 19 September 2012)

The kinetic properties of the pressure-driven Poiseuille flow in nanochannels with and without nanoparticles were studied with a nonequilibrium molecular dynamics simulation. To allow the fluid to dissipate heat, the boundary was kept at a constant temperature. Pure fluid simulations were taken as references and also used to study the fluid-wall interfacial interaction effects. The viscosity profiles of the fluid were calculated on the basis of velocity profiles and known applied shear stress. We present the relationship between the viscosity increase and particle loading. The role of channel wall–fluid wetting properties on the flow and viscosity was also investigated.

DOI: 10.1103/PhysRevE.86.036313 PACS number(s): 47.60.Dx, 31.15.at, 47.57.E−

I. INTRODUCTION

Nanoparticle suspension (nanofluid) has been an area of ongoing interest since it was proposed by Choi [1] in the 1990's for thermal management applications. Usually, the nanoparticles are made of metal or nonmetal materials, while water, alcohols, and oils are typically applied as the base fluid. Most of the work on nanofluids has focused on the thermal properties due to the promise of heat transfer enhancement [2–4]. Keblinski [5] proposed a number of potential factors responsible for the anomalous increase in nanoparticle suspension heat conduction. A larger body of subsequent research established that particle clustering is the only reasonable mechanism behind large thermal conductivity increases, while with well dispersed particles, conductivity increases are moderate and require large particle loading to achieve a significant effect. However, clustering and large particle loadings are expected to lead to significant viscosity increases, thus questioning the usefulness of nanofluids.

Studies of the kinetic properties of nanofluids are less prominent than those of thermal conductivity. However, they are critical in determining the heat transfer coefficient. The experiments of Wang [6] and Das [7] showed that the particle volume fraction played a critical role in the effective viscosity of the nanoparticle suspension. The rheological properties of alumina nanoparticles dispersed into a base water fluid were measured by Annop to study the effect of an electrical double layer [8].

Atomic-level modeling work on the kinetic properties of pure fluid has a substantial history. Koplik [9] established a nonslip boundary model to observe the velocity of a Lennard-Jones (LJ) fluid and presented the classic parabolic distribution of the velocity field at a small Reynolds number. "Method of planes" (MOP, a formulation of the Irving-Kirkwood procedure [10,11] in reciprocal space that greatly simplifies the calculation of momentum and energy fluxes) technology was applied to the Poiseuille flow simulations by Daivis. To remove viscous flow-generated heat, Fried [12] kept the temperature of the walls constant. He also compared the molecular dynamics (MD) simulation results with those calculated by computational fluid dynamics (CFD) software, and demonstrated that the fluid density, velocity, and pressure distributions obtained via MD fit the continuum-equations-based CFD results very well. The Poiseuille flow simulations received the attention of numerous researchers [13–20], who studied the macroscopic viscosity of pure fluids under a constant shear rate.

By contrast, MD simulations of the shear flow of fluid-particle suspensions are lacking. The theoretical framework for understanding suspension viscosity is provided by the Einstein [21] model and the Batchelor [22] model. They are widely applied to calculate the global effective viscosity of a dilute suspension. In this paper, the viscous flow properties of the nanoparticle suspension obtained with the molecular dynamics method are reported and compared against those characterizing pure fluid. We make efforts to study the local viscosity and effects of the channel wall–fluid interfacial interaction on the flow characteristics.

The structure of this paper is as follows. In the next section, we will describe our model structures and simulation methodology. Section III presents simulation results on the kinetics of fluid flow in a nanosized channel both for pure fluid and nanoparticle suspension. Finally, Sec. IV includes a summary and conclusion.

II. MODEL STRUCTURES AND SIMULATION METHODOLOGY

The initial structure is set up as shown in Fig. 1. The nanoparticle suspension is confined between two parallel planes formed by "solid" atoms arranged as an fcc lattice. The simulation cell sizes are $L_x = L_y = 15\sigma \times 15\sigma$ (in x and y in-layer directions) and $L_z = 50\sigma$, where 8586 fluid atoms with a density of $0.85/\sigma^3$ are confined between 1600 boundary atoms, each of which has the same size as the fluid atom. Here, σ is the length scale parameter of the interatomic potential. In addition, spherical particles composed of solid atoms are dispersed randomly in the fluid. Here, the particle is made via a spherical cut of atoms arranged on an fcc lattice. Each nanoparticle has a radius of 2σ and contains 44 atoms that have the same size as that of the solid wall and fluid atoms. Periodic boundaries are applied in both the x and y dimensions. Since the upper and lower walls are not moving relative to each other, we used just one solid region for both

*Corresponding authors': wemma7@gmail.com, zqchen@seu.edu.cn

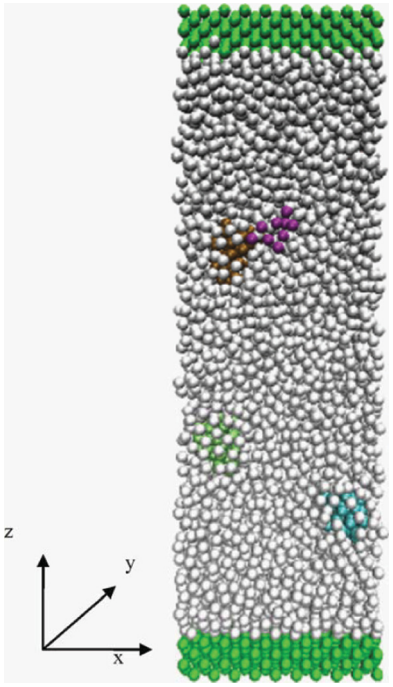

FIG. 1. (Color online) The geometry of the simulation structure.

walls. This allowed us to use periodic boundary conditions in the direction that is also normal to the wall. Such a choice makes the pressure equilibration easy and does not require any constraints to be placed on the wall atoms.

The truncated Lennard-Jones potential governs all atomic interactions:

$$V_{\mathrm{LJ}}(r) = 4\varepsilon\left[\left(\frac{\sigma}{r}\right)^{12} - \left(\frac{\sigma}{r}\right)^{6}\right], \tag{1}$$

where r is the interatomic spacing, while σ and ε are the length and energy scale parameters, respectively. The cutoff distance is 3.0σ. The strengths of the interactions between the solid wall atoms and between atoms within each particle ε_{ss},ε_{pp} are nine times larger than those between the liquid atoms ε_{ll}. ε_{ll} is taken as the reference energy and is equal to unity. Here, the subscripts l, s, and p are used to indicate liquid, solid, and particle, respectively. The strengths of the interactions between liquid and solid wall or liquid and particle ε_{sl} and ε_{pl} are equal to $3\varepsilon_{ll}$, obeying to the Lorentz-Berthelot combining rule [23],

$$\begin{aligned} \sigma_{1-2} &= (\sigma_1 + \sigma_2)/2, \\ \varepsilon_{1-2} &= (\varepsilon_1 \cdot \varepsilon_2)^{1/2}. \end{aligned} \tag{2}$$

The strength of the interactions between the solid wall and particle atoms ε_{sp} is $3\varepsilon_{ll}$. This choice of interaction corresponds to a hydrophilic interface. In addition, we performed simulations using $0.2\varepsilon_{ll}$ as the strengths of the interaction between the wall and fluid atoms to model a hydrophobic interface.

Throughout the simulations, the solid atoms were allowed to exhibit full dynamics with no constraints (or springs attaching the atoms to a fixed position). The fcc solid structure was maintained naturally due to a strong solid-solid attractive LJ potential.

The nonequilibrium molecular dynamics method is used to carry out the simulations. The system is equilibrated at a

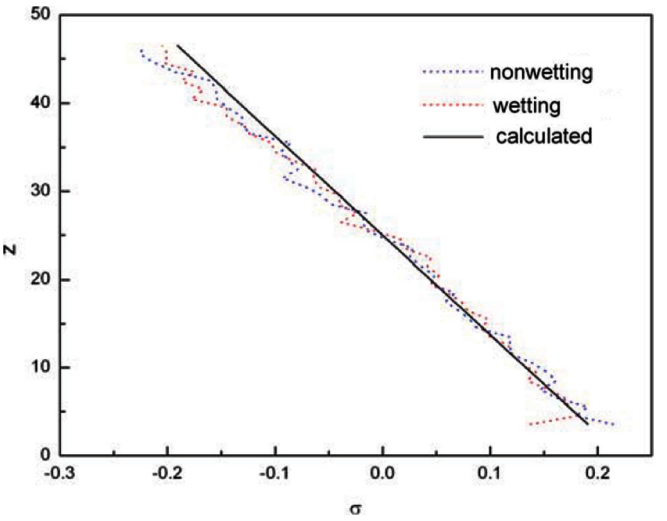

FIG. 2. (Color online) The virial stress distribution of pure fluid with wetting and nonwetting walls. The solid line is calculated from the total body force divided by the area as described in the text.

constant pressure and reduced temperature $T^* = kT/\varepsilon_{ll} = 0.8$, i.e., above the melting point of the LJ fluid. We verify that the velocity distribution obeys the Maxwell distribution after 500000 MD time-step runs, indicating that the equilibrium is well established. The equation of motions, governed by Newton's law, is integrated by a Verlet algorithm with a time step of 0.002τ, where $\tau = (m\sigma^2/\varepsilon)^{1/2}$ is the LJ time unit [24].

To induce flow, we apply force uniformly to all atoms in the liquid to mimic the Poiseuille flow driven by a pressure drop. Considering that the atomic density of the liquid is uniform, we know precisely how much force is applied to a slab of a liquid of an arbitrary thickness centered at the channel center. This force is equal to the volume of the slab times the atomic density times the force added to each atom. This applied body force in a steady-state flow has to be balanced by a shear (surface) force. This allows us to calculate the shear stress directly by dividing the total body force on the slab by the area of the surface delimiting the slab.

We verified that such a calculated stress is within the same statistical error as that calculated via molecular virial stress definitions. As seen in Fig. 2, the shear stress component is within the statistical fluctuation, the same for wetting and

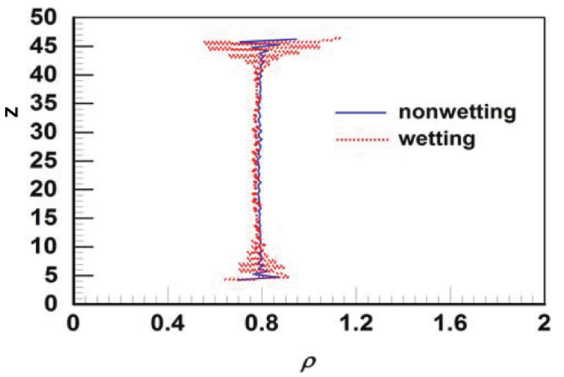

FIG. 3. (Color online) The density distribution of fluid along the z dimension with wetting and nonwetting walls.

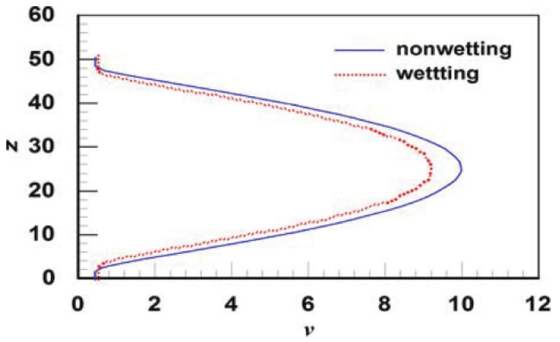

FIG. 4. (Color online) The velocity distribution of pure fluid with wetting and nonwetting walls.

nonwetting walls, and can be well represented as a linear function of the z coordinate with a zero value at the center of the channel. This follows directly from the fact that the total body force is proportional to the slab volume, i.e., its thickness, and, as discussed above, from the force balance consideration, it has to be equal to the shear force.

While a uniform force is added to the liquid atoms, an opposite force that has the same value as the one added to the liquid is subtracted from the boundary's atoms. Consequently, the total net momentum of the whole system is zero. Such a procedure does not require placing constraints on the wall atoms. The only difference in this method with respect to the traditional view of the Poiseuille flow is a different frame of reference, which will not impact any viscosity results. Throughout the simulations, the solid walls are kept at a constant temperature via simple velocity rescaling. However, the center-of-mass motion of the wall was subtracted before the rescaling procedure and added back after the rescaling, so that the flow-generated heat due to the shear can be dissipated into the ambient atmosphere via heat transfer with the solid walls, thus avoiding a significant temperature increase.

The "production runs" continue for around 1 000 000 time steps for the flow to reach the steady state, where the velocity profiles are fully developed. Based on the velocity profiles we can calculate the viscosity via the definition

$$\eta_z = -\frac{\langle P_{xz}\rangle}{\frac{\partial v_x}{\partial z}}, \tag{3}$$

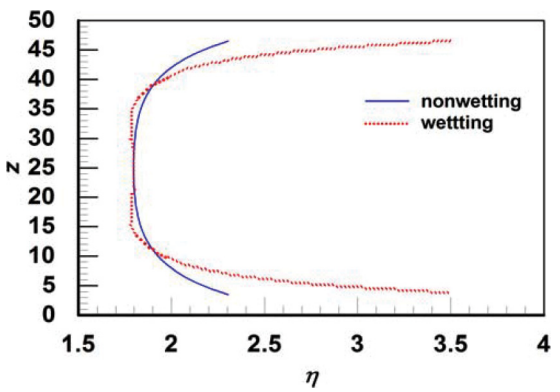

FIG. 5. (Color online) The local viscosity of pure fluid with wetting and nonwetting walls.

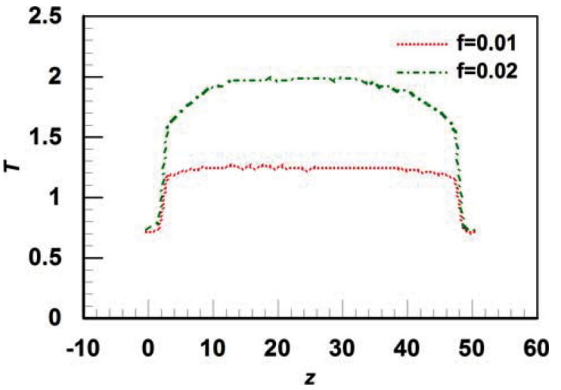

FIG. 6. (Color online) The temperature profile with different driving forces (f denotes the reduced driving force).

where, indicating the viscosity, P_{xz} is the shear component of the pressure tensor, and v is the velocity. In our simulations, shear stress is added along the x dimension, and the gradient (including temperature, velocity, and viscosity gradients) occurs only in the z direction. To reduce the noise level in the determination of the viscosity, we first fit the velocity profile with sixth-order polynomials that are symmetric about the center of the channel and take an analytical derivative to obtain the velocity gradient. The shear stress component is represented as a linear function of the z coordinate with the zero value at the center of the channel (see Fig. 2).

III. SIMULATION RESULTS AND ANALYSIS

The simulations of pure fluid flow in a nanosized channel are carried out to establish a reference and to investigate the effects of the wall-fluid interactions. Both hydrophilic and hydrophobic walls are applied, and the average driving force on every fluid atom is 0.01 in reduced units.

The fluid density distribution along the z dimension is showed in Fig. 3. The fluid density near the wetting wall shows an oscillation phenomenon that extends to a distance of three to four times of the atom's diameter, resulting from the strong interaction between the fluid atoms and solid wall atoms. This is in accord with previous research findings [25,26]. For a nonwetting (hydrophobic) interface, the layering is not as well developed and does not extend significantly into the liquid.

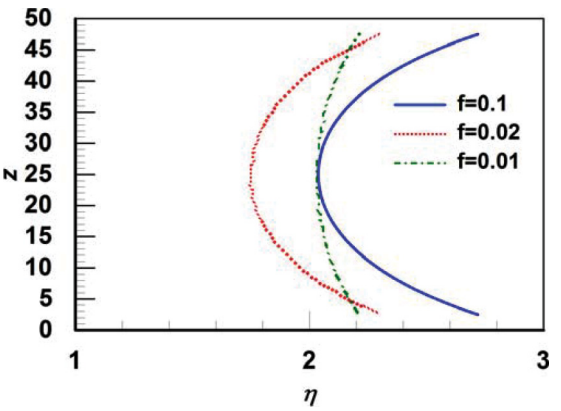

FIG. 7. (Color online) The local viscosity of pure fluid with various driving forces (f denotes the reduced driving force).

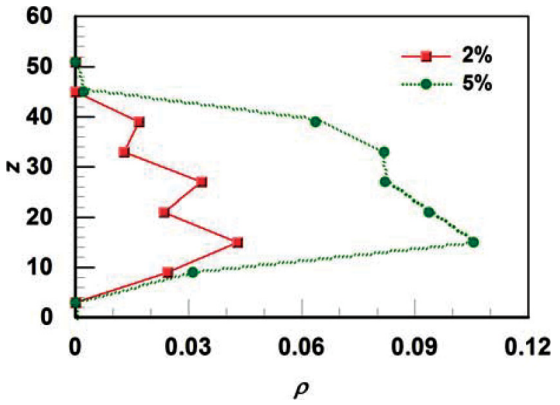

FIG. 8. (Color online) The density distribution of nanoparticles along the z dimension.

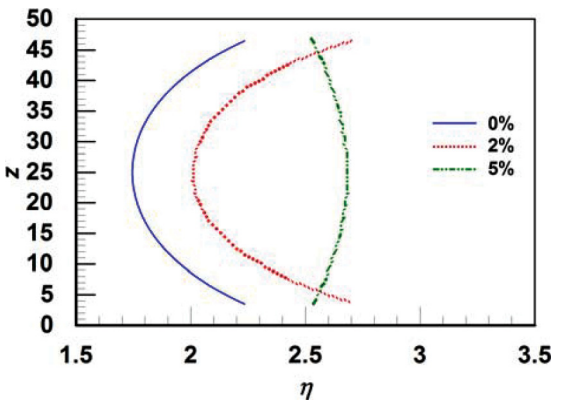

FIG. 10. (Color online) The local viscosity of nanoparticle suspension with various particle volume fractions along the z dimension.

Fluid velocity distribution profiles are show in Fig. 4. The velocity profiles for both wetting and nonwetting walls are parabolic, which is consistent with the result of macroscopic theory. The higher overall velocity range in the case of the nonwetting wall can be explained by a lower local viscosity near the wall, as we discuss below.

The local viscosity calculated from formula (3) and sixth-order polynomial fitting to the velocity profile is presented in Fig. 5. The data show almost the same viscosity in the center of the channel for both wetting conditions, but near the walls the viscosity increases, with a particularly large increase for the wetting wall. This phenomenon demonstrates that fluid atoms of the layer nearest to the walls are locked to the boundaries by adhesive interactions, and thus impede the fluid's flow. This effect is naturally more pronounced in the case of a wetting interface.

We investigate the effect of the driving force on the fluid velocity and temperature. It is expected that, due to an increased rate of heat generation, the larger the driving force, the higher is the temperature. This can be observed in the temperature profiles in Fig. 6. Here, the nonwetting interface is studied to enhance temperature changes due to the interfacial thermal resistance which leads to temperature jumps at the liquid-solid interfaces. When the driving force is doubled, the larger viscous heat generated by the shear may not be transferred to the walls as efficiently, so the interior fluid is much warmer. As a consequence, the viscosity for the stronger driven fluid, which is warmer, is smaller, as shown in Fig. 7.

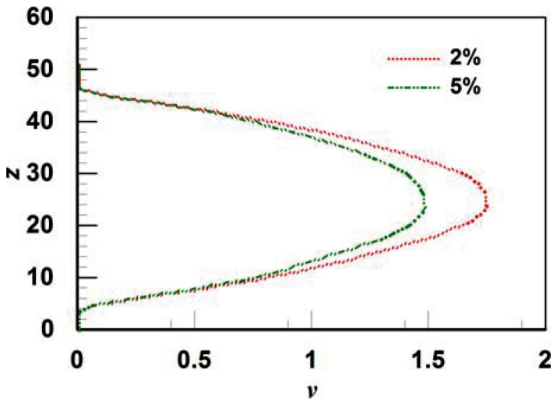

FIG. 9. (Color online) The velocity distribution of nanoparticle suspension along the z dimension.

To study the effect of particle addition on fluid properties, we investigate fluids with 2% and 5% particles by volume. In each case a force of 0.02 is added to every fluid atom, and the particles are spherically shaped with a radius of 2.

The particle atom density profiles are presented in Fig. 8. As clearly seen in the figure, particularly for 5% suspension, the particle concentration is higher in the central part of the fluid. The particles are likely driven to the center by the fact that the velocity gradient there is zero (see Fig. 9). As a consequence, the particle associated with the higher local viscosity has a less detrimental effect on the fluid flow.

In Fig. 10, we present local viscosity for pure fluids and suspensions. In the case of a 2% suspension, the local viscosity is a little larger than that of a pure fluid at corresponding locations, however, in both cases, the local fluid viscosity near the wall is larger than that in the interior fluid. When the particle volume fraction increases to 5%, the viscosity is much larger and in fact has a maximum at the center of the channel. This indicates that with high particle loadings, the particle-related viscosity increase dominates over the wall effects.

IV. CONCLUSION

Kinetic properties, especially the viscosity of pure fluid and nanoparticle suspensions flowing in nanochannels, were studied with the molecular dynamics method. We demonstrated that the adhesive interaction between walls and fluid atoms plays a significant role in the fluid's viscosity due to the solidlike structure acquired by the fluid near the channel walls. Owing to stronger interactions, this effect is particularly significant in the case of the wetting interface.

Moderate particle loading leads to an overall viscosity increase, however, the viscosity remains higher near the walls. With larger particle loadings, the viscosity increase is significantly larger and the maximum viscosity in the center of the channel is larger, too. This is caused by the fact that nanoparticles are driven to the center as they reside in the region of low shear stress. It is also possible that large particle loadings lead to the partial destruction of the interfacial layer, which, as a consequence, diminishes the wall effect on the viscosity.

ACKNOWLEDGMENT

This work was supported by the National Basic Research Program of China (No. 2006CB300404), National Science Foundation of China (No. 51276041) and the International Science and Technology Cooperation Technical Exchange Project of the Ministry of Science and Technology (No. 2011DFA60290).

[1] S. U. S. Choi, in *Developments and Applications of Non-Newtonian Flows*, edited by D. A. Siginer and H. P. Wang (ASME, New York, 1995), pp. 99–105.
[2] T. Hong, H. Yang, and C. J. Choi, J. Appl. Phys. **97**, 064311 (2005).
[3] R. L. Hamilton and O. K. Crosser, Ind. Eng. Chem. Fundamen. **1**, 187 (1962).
[4] P. M. Hui, X. Zhang, A. J. Markworth, and D. Stroud, J. Mater. Sci. **34**, 5497 (1999).
[5] P. Keblinski, S. R. Phillpot, S. U. S. Choi, and J. A. Eastman, Int. J. Heat Mass Transfer **45**, 855 (2002).
[6] X. Wang, X. Xu, and S. U. S. Choi, J. Thermophys. Heat Transfer **13**, 474 (1999).
[7] S. K. Das, N. Putra, and W. Roetzel, Int. J. Heat Mass Transfer **46**, 851 (2003).
[8] K. B. Anoop, S. Kabelac, T. Sundararajan, and S. K. Das, J. Appl. Phys. **106**, 034909 (2009).
[9] J. Koplik, J. R. Banavar, and J. F. Willemsen, Phys. Rev. Lett. **60**, 1282 (1988).
[10] B. D. Todd, P. J. Daivis, and D. J. Evans, Phys. Rev. E **51**, 4362 (1995).
[11] B. D. Todd, D. J. Evans, and P. J. Daivis, Phys. Rev. E **52**, 1627 (1995).
[12] J. Fried, Master's thesis, Virginia Polytechnic Institute and State University, 2007.
[13] W. T. Ashurst and W. G. Hoover, Phys. Rev. A **658** (1975).
[14] A. W. Lees and S. F. Edwards, J. Phys. C **5**, 1921 (1972).
[15] D. J. Evans and G. P. Morriss, Phys. Rev. A **30**, 1528 (1984).
[16] G. Ciccotti, G. Jacucci, and I. R. McDonald, J. Stat. Phys. **21**, 1 (1979).
[17] K. Singer, J. V. L. Singer, and D. Fincham, Mol. Phys. **40**, 515 (1980).
[18] W. G. Hoover, Annu. Rev. Phys. Chem. **34**, 103 (1983).
[19] D. Brown and J. H. R. Clarke, Phys. Rev. A **34**, 2093 (1986).
[20] D. J. Evans and G. P. Morriss, *Statistical Mechanics of Nonequilibrium Liquids* (Academic, London, 1990).
[21] A. Einstein, *Investigations on the Theory of the Brownian Movement* (Dover, New York, 1956).
[22] G. K. Batchelor, J. Fluid Mech. **83**, 97 (1977).
[23] J. Delhommelle and P. Millie, Mol. Phys. **99**, 619 (2001).
[24] M. P. Allen and D. J. Tildesley, *Computer Simulation of Liquids* (Clarendon, Oxford, UK, 1987).
[25] D. Poulikakos, S. Arcidiacono, and S. Maruyama, Microscale Thermophys. Eng. **7**, 181 (2003).
[26] M. Heuberger, M. Zäch, and N. D. Spencer, Science **292**, 905 (2001).